Upconverting Nanoparticles Prompt Remote Near-Infrared Photoactivation of Ru(II)-Arene Complexes

Upconverting Nanoparticles Prompt Remote Near Infrared Photoactivation of Ru(II) Arene Complexes

Emmanuel Ruggiero,[a] Claudio Garino,[b] Juan C. Mareque-Rivas,[a, c] Abraha Habtemariam*[a, c, d] and Luca Salassa*[a, e]

[a] E. Ruggiero, Prof. J. C. Mareque-Rivas, Dr. A. Habtemariam, Dr. L. Salassa, CIC biomaGUNE Paseo de Miramón 182, 20009, Donostia – San Sebastián, Euskadi, Spain. E-mail: a.habtemariam@warwick.ac.uk, lsalassa@cicbiomagune.es.

[b] Dr. C. Garino, Department of Chemistry and NIS Centre of Excellence, University of Turin, via Pietro Giuria 7, Turin 10125, Italy.

[c] Prof. J. C. Mareque-Rivas, Dr. A. Habtemariam, IKERBASQUE, Basque Foundation for Science, Bilbao 48011, Spain.

[d] Dr. A. Habtemariam, Department of Chemistry, University of Warwick, Coventry CV4 7AL, United Kingdom.

[e] Dr. L. Salassa, Kimika Fakultatea, Euskal Herriko Unibertsitatea and Donostia International Physics Center (DIPC), P.K. 1072 Donostia – San Sebastián, Euskadi, Spain.

Abstract

The synthesis and full characterization (including X-ray diffraction and DFT calculations) of two new piano-stool Ru(II) arene complexes, namely [(η^6-*p*-cym)Ru(bpy)(*m*-CCH-Py)][$(PF)_6]_2$ (**1**) [(η^6-*p*-cym)Ru(bpm)(*m*-CCH-Py)][$(PF)_6]_2$ (**2**) (*p*-cym = *p*-cymene, bpy = 2,2'-bipyridine, bpm = 2,2'-bipyrimidine, and *m*-CCH-Py = 3-ethynylpyridine) is described and discussed. Reaction of the *m*-CCH-Py ligand of **1** and **2** with diethyl-3-azidopropyl phosphonate by Cu-catalysed click chemistry affords [(η^6-p-cym)Ru(bpy)(P-Trz-Py)][$(PF)_6]_2$ (**3**) and [(η^6-p-cym)Ru(bpm)(P-Trz-Py)][$(PF)_6]_2$ (**4**) (P-Trz-Py = [3-(1-Pyridin-3-yl-[1,2,3]triazol-4-yl)-propyl]-phosphonic acid diethyl ester). Upon 395-nm light excitation, **1**–**4** photodissociate the monodentate pyridyl ligand forming the aqua adducts [(η^6-*p*-cym)Ru(bpy)$(H_2O)]^{2+}$ and [(η^6-*p*-cym)Ru(bpm)$(H_2O)]^{2+}$. Tm-doped upconverting nanoparticles (UCNPs) are functionalized with **4** exploiting their surface affinity for phosphonate group of the complex. The so-obtained nanosystem **UCNP@4** undergoes NIR photoactivation at 980 nm, producing the corresponding reactive aqua species, which binds the DNA model base guanosine 5′-monophosphate.

Introduction

Encouraged by the clinical success of photodynamic therapy (PDT),[1] light-activatable molecules and nanomaterials are being increasingly investigated for their capacity to generate *in situ* biologically active species with high spatio-temporal control. In principle, such an attractive strategy allows localizing the biological effects of drugs, potentially reducing their therapeutic drawbacks. For this reason, light activation has found application in a number of fields, and diverse systems have been designed as neuroscience tools,[2] drug delivery platforms[3,4] and anticancer prodrugs.[5,6]

Promising metal-based photo-chemotherapeutics have been developed exploiting the unique photochemical and antitumoral properties of transition metal complexes. Several research groups worldwide have demonstrated that light-activatable complexes of various transition metals (e.g. Pt, Ru, Rh, Ir) show encouraging antineoplastic profiles and unconventional mechanisms of action compared to their ground-state analogues.[4,5,6,7]

Nevertheless, the poor absorption properties of metal complexes in the therapeutic window of the red and near infrared (NIR) spectrum (ca. 600–1000 nm) pose a serious limitation for further advancing their use towards preclinical and clinical studies as maximal light penetration into tissues is achieved in this wavelength range, and damage to biological components is minimized.[8,9] Compared to PDT photosensitizers, photoactivatable anticancer metal complexes generally display low-energy absorption bands that rarely extend over 550 nm and have modest extinction coefficients. Although a few exceptions have been reported,[10,11,12] it is extremely challenging to improve absorption features without altering ground-state stability and photoreactivity in metal complexes.

For this reason, we and other groups have recently started exploring the use of upconversion nanoparticles (UCNPs) as phototriggers for near infrared photoactivation of (anticancer or not) metal complexes.[9,13,14,15,16,17,18,19,20] UCNPs are typically $NaYF_4$ or $NaGdF_4$ nanocrystals doped with lanthanide ions such as Yb^{3+}:Tm^{3+} or Yb^{3+}:Er^{3+}, which convert NIR light (980 nm) into UV-vis light via multiphotonic processes.[21,22] Conveniently, UV-vis photons emitted by UCNPs upon NIR light excitation can promote photochemical reactions in metal complexes and potentially switch on their biological effects. Ford and coworkers showed that NIR irradiation of UCNPs loaded with either the Roussin's black salt anion or the photoCORM *trans*-[Mn(2,2'-bipyridine)$(PPh_3)_2(CO)_2$] results in the release of NO and CO, respectively.[13,14] Similarly, we have demonstrated that related upconversion nanosystems promoted the release of pyridine from a ruthenium polypyridyl complex[16] and the generation of Pt(II) species from a Pt(IV) prodrug candidate.[17] Instead, Shuqing He et al. designed an UCNP-system capable of releasing doxorubicin in a controlled fashion, by taking advantage of a photoactivatable Ru complex which acts as a valve.[20] Differently, Bonnet and coworkers also reported a promising system for activation at 630 nm of a model Ru polypyridyl complex using triplet-triplet annihilation upconversion.[23]

The unique optical (upconversion emission) and chemical (e.g. Gd^{3+} and $^{18}F^-$ on the surface) features of UCNPs are also exploited for multimodal imaging (SPECT/PET,[24,25] CT,[26] MRI,[27] optical[28] and photoacustic[29]) as demonstrated by numerous *in vivo* studies, which have appeared in the last few years. These properties, together with the low toxicity of UCNPs,[30] make hybrid nanomaterials based on UCNPs and metal complexes suitable for application in theranostics.[31]

In this contribution, we devise a new approach to demonstrate the usefulness of UCNPs in the photoactivation of ruthenium(II) arene complexes, an attractive class of metal complexes with remarkable *in vitro*[32,33] and *in vivo*[34] anticancer activity.

Pyridinato Ru(II)-arene derivatives display dark-stability and selectively release pyridinato ligands upon visible light excitation, to generate highly reactive aqua species.[35,36,37] Controlling such reaction is key to activate the biological activity of Ru(II)-arene derivatives.

For this purpose, we prepared two new Ru-pyridinato derivatives, namely [(η^6-*p*-cym)Ru(bpy)(*m*-CCH-Py)][$(PF)_6]_2$ (**1**) and [(η^6-*p*-cym)Ru(bpm)(*m*-CCH-Py)][$(PF)_6]_2$ (**2**) (where *p*-cym = *p*-cymene, bpy = 2,2'-

bipyridine, bpm = 2,2'-bipyrimidine, and *m*-CCH-Py = 3-ethynylpyridine) and exploited a click chemistry strategy to derivatize the monodentate 3-ethynylpyridine arm with a phosphonate group, which has high affinity for the UCNP surface.[38] The functionalized complexes (**3** and **4**), together with their precursors were characterized and their photochemistry studied in detail using different methods, including Density Functional Theory (DFT).

On the basis of its photoreactivity, complex **4** was selected for anchoring onto core@shell $NaYF_4$:Yb(30%)/Tm(0.5%)@$NaYF_4$ nanoparticles and performing NIR photochemistry experiments.

Results proved the obtained **UCNP@4** nanoconstruct is activated under 980-nm irradiation to generate the reactive aqua photoproducts $[(\eta^6\text{-}p\text{-cym})Ru(bpm)(H_2O)]^{2+}$, which binds the DNA model base guanosine 5′-monophosphate (GMP).

The synthetic strategy and NIR photoactivation reported herein may offer new intriguing opportunities for the design of innovative prodrug nanosystems, relying on the rich anticancer properties of metallo-arene complexes.

Results and Discussion

Synthesis of Complexes 1–4 and UCNP@4

Complexes $[(\eta^6\text{-}p\text{-cym})Ru(bpy)(m\text{-CCH-Py})][(PF)_6]_2$ (**1**) and $[(\eta^6\text{-}p\text{-cym})Ru(bpm)(m\text{-CCH-Py})][(PF)_6]_2$ (**2**) were synthesized in moderate yields (ca. 35%) treating the precursors $[(\eta^6\text{-}p\text{-cym})Ru(bpy)Cl][PF_6]$ and $[(\eta^6\text{-}p\text{-cym})Ru(bpm)Cl][PF_6]$ with $AgNO_3$ and subsequently performing ligand exchange reactions with 3-ethynylpyridine in MeOH/H_2O (Scheme 1A).[39,40,41,42] A range of techniques was then used to characterize both complexes, including X-ray, multinuclear NMR, mass spectrometry and elemental analysis.

We employed 3-ethynylpyridine since pyridyl ligands are known to render Ru-arene complexes hydrolytically stable in the dark.[35,36,37] Moreover, the presence of an alkyne group on the ligand allowed adopting click chemistry for the functionalization of **1** and **2** and anchoring onto UCNPs. Click chemistry is a convenient strategy for ligand design in inorganic chemistry and has attracted significant attention in recent years.[43] Such an approach affords (bio)orthogonal reactions that are high yielding, selective and robust under mild conditions.[44]

Inspired by the work of Branda and co-workers,[45] we employed diethyl-3-azidopropyl phosphonate and its azido function to incorporate the phosphonate group into **1** and **2** via click chemistry. Phosphonates have good affinity for the $NaYF_4$ surface of UCNPs and improve their biocompatibility as demonstrated by various groups.[38,46]

Diethyl-3-azidopropyl phosphonate was obtained reacting (3-bromopropyl) phosphonic acid with sodium azide in acetone.[47] Clicked complexes $[(\eta^6\text{-p-cym})Ru(bpy)(P\text{-Trz-Py})][(PF)_6]_2$ (**3**) and $[(\eta^6\text{-p-cym})Ru(bpm)(P\text{-Trz-Py})][(PF)_6]_2$ (**4**) (where P-Trz-Py = [3-(1-Pyridin-3-yl-[1,2,3]triazol-4-yl)-propyl]-phosphonic acid diethyl ester) were hence prepared reacting respectively **1** and **2** with diethyl-3-azidopropyl phosphonate in THF/water at 60 °C for 72 h in the presence of $CuSO_4$ and sodium ascorbate (Scheme 1A). Complexes **3** and **4** were obtained in good yields and purity and characterized by ^1H ^{13}C and ^{31}P NMR spectroscopy and mass spectrometry.

Although the photochemical behaviour of the complexes is rather similar (*vide infra*), **4** was selected for loading onto core@shell $NaYF_4$:Yb^{3+}/Tm^{3+}@$NaYF_4$ UCNPs on the basis of the higher reactivity of its bpm analogue **2** compared to **1** (bpy). For this reason, we first activated the phosphonate group of **4** into its acid form by de-esterification with tribromo(methyl)silane (TMSBr) in CH_2Cl_2. Next, the so-obtained complex was stirred overnight with oleate-free core@shell UCNPs in H_2O, and an orange pellet corresponding to **UCNP@4** was collected after several washing and centrifugation steps (Scheme 1B). Characterization of the hybrid material was achieved using a combination of different techniques (*vide infra*).

Scheme 1. .Schematic representation of the approaches employed for the synthesis of (A) **1**–**4** and (B) **UCNP@4**.

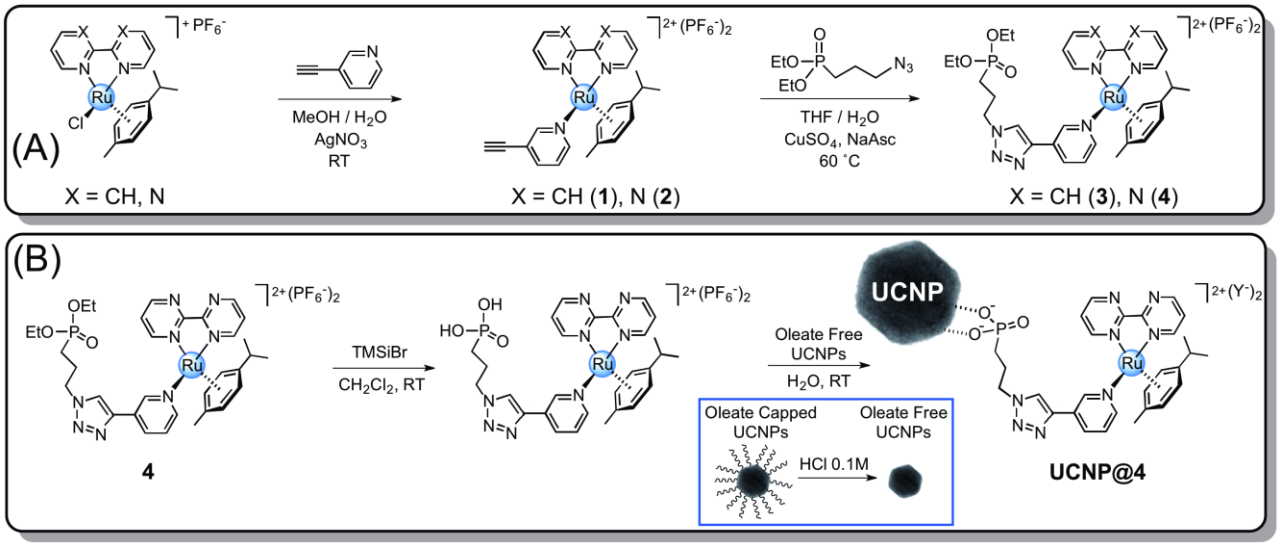

Characterization and Photochemical Properties of 1 and 2

X-ray and DFT structures. The crystal structure of the hexafluorophosphate salts of **1** and **2** were determined by X-ray diffraction and are shown in Figure 1. These structures are fairly similar, and first-coordination spheres of both Ru complexes display comparable bond distances and angles (Table 1). Complexes **1** and **2** present the typical piano-stool geometry of related Ru^{II} arene complexes with N,N' ancillary ligands.[41] Crystal packing and experimental details including X-ray data are reported in the Supporting Information (Table S1 and Figure S1 and S2). DFT-optimized ground-state geometries (Table 1, B3LYP/LanL2DZ/6-31G**) for **1** and **2** describe satisfactorily the structure of the complexes. Calculated and experimental Ru–N bonds differ only by < 0.02 Å. Ru–*p-cym*(centroid) distances are, however, ca. 0.15 Å longer in the DFT calculations compared to X-ray determinations.

Two triplet excited-state structures were also DFT-minimized for both **1** and **2** (Table 1), since triplets are likely to be involved in the photochemistry of the complexes. The lowest-lying triplets (T0) for both compounds have a distorted structure with one Ru−N(N,N′) bond strongly elongated (> 2.40 Å). However, the higher-energy triplet geometries (T1) display elongated Ru−N(m-CCH-Py) distances (> 2.51 Å).

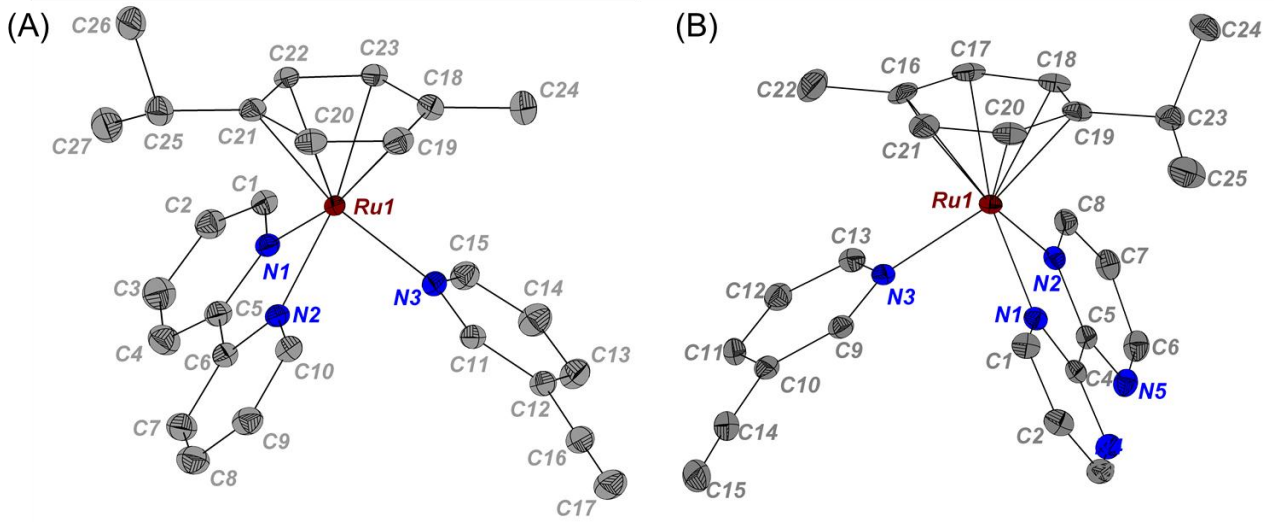

Figure 1. Crystal structures of (A) **1** and (B) **2**. Thermal ellipsoids are depicted at the 50% probability level. Counter ions (PF_6^-) and H atoms are omitted for clarity.

Table 1. Selected X-ray and DFT-calculated bond lengths [Å] for 1 and 2 in the ground-state (S0) and in two triplet-state (T0 and T1) geometries.

Compound	Ru−N(*m*-CCH-Py)	Ru−N(N,N′)	Ru−N(N,N′)	Ru−*p*-cym$_{(centroid)}$
		X-Ray		
1	2.125(2)	2.085(2)	2.084(2)	1.701
2	2.1241(17)	2.0995(16)	2.0873(16)	1.704
		Ground State (S0)		
1	2.159	2.103	2.095	1.848
2	2.158	2.111	2.106	1.850
		Lowest-lying Triplet State (T0)		
1	2.164	2.404	2.113	2.079
2	2.143	2.457	2.131	2.082
		Triplet State (T1)		
1	2.556	2.087	2.082	2.157
2	2.511	2.093	2.113	2.140

Photophysical and photochemical properties of 1 and 2. The UV-vis spectrum (Figure S3) of **1** exhibits five distinct bands, at 245 nm (ε = 7600 $M^{-1}cm^{-1}$), 269 nm (ε = 6400 $M^{-1}cm^{-1}$), 305 nm (ε = 5400 $M^{-1}cm^{-1}$), 317 (ε = 5700 $M^{-1}cm^{-1}$) and 370 nm (ε = 1300 $M^{-1}cm^{-1}$), while **2** (Figure 2A) displays two major bands and one shoulder, respectively at 246 nm (ε = 3700 $M^{-1}cm^{-1}$), 370 nm (ε = 1200 $M^{-1}cm^{-1}$) and 291 nm (ε = 3200 $M^{-1}cm^{-1}$). TD-DFT is a valuable tool to assign the character of the absorption bands. Calculation of singlet-singlet transitions and analysis of their orbital composition (Table S2 and S3, and Figure S4) provide information on the nature of the singlet-excited states, which can be conveniently visualized through electron density difference maps (EDDMs, Figure S5 and S6).

In agreement with related complexes, the high-energy bands of **1** and **2** have mixed MLCT (metal-to-ligand charge transfer) and intra-ligand character (< 325 nm). Conversely the lowest- energy bands are mainly MLCT. Furthermore, transitions of weak intensity with mixed MLCT/MC (metal centred) character are present in their tail. These latter transitions have significant contribution from σ-antibonding orbitals, which confer them a dissociative nature (Figure S4). Through generation of these dissociative singlet states and subsequent intersystem-crossing, the low-energy triplets T0 and T1 (Figure 2B) can be populated. T1 is dissociative towards the 3-ethynylpyridine ligand, whereas T0 might promote the partial dissociation of a pyridyl ring of the bpy/bmp ligand (Figure S7–S9). Nevertheless, release of the chelating ligands is prevented by the strong coordination of the second ring. For this reason, light excitation of **1** and **2** results in selective photodissociation of the monodentate 3-ethynylpyridine ligand. Figure 2B (Figure S10 for **1**) reports the energy level of selected singlet and triplet states for **2**, together with their corresponding EDDMs (singlets) and spin densities (triplets).

The low energy of the T0 state (1.33 and 1.29 eV for **1** and **2**, respectively) calculated by DFT and the small energy difference between this state and T1 are consistent with the lack of emission from the two complexes, which tend to relax to the ground state via non-radiative pathways, and with their modest photodissociation quantum yields <1% as determined by actinometry methods[48] (Φ_1 = 0.003 and Φ_2 = 0.008, Table S4 and Figure S11–S14).

Figure 2C and 2D show the photolysis of **2** (D_2O:DMSO-d_6, 95:5%) upon 395-nm light irradiation (15 $mW \cdot cm^{-2}$) followed by UV-vis and ^1H NMR spectroscopy. Light irradiation induces variations in UV-vis absorption profile of **2**, with a decrease at 370 nm and an increase in the 260−320 nm region of the bands. The presence of isosbestic points at 230 and 315 nm reveals the formation of a single photoproduct. Furthermore, diagnostic changes in the ^1H NMR spectra of **2**, as well as UPLC-MS analysis (Figure S15), clearly confirm the release of 3-ethynylpyridine and formation of the aqua species [(η^6-*p*-

cym)Ru(bpm)(H_2O)]$^{2+}$.[35,36,37] A control experiment indicates **2** is stable in the dark up to at least 24 h (Figure S16). Analogue results were observed for **1** and are summarized in Figure S17, S18 and S19 of the Supporting Information.

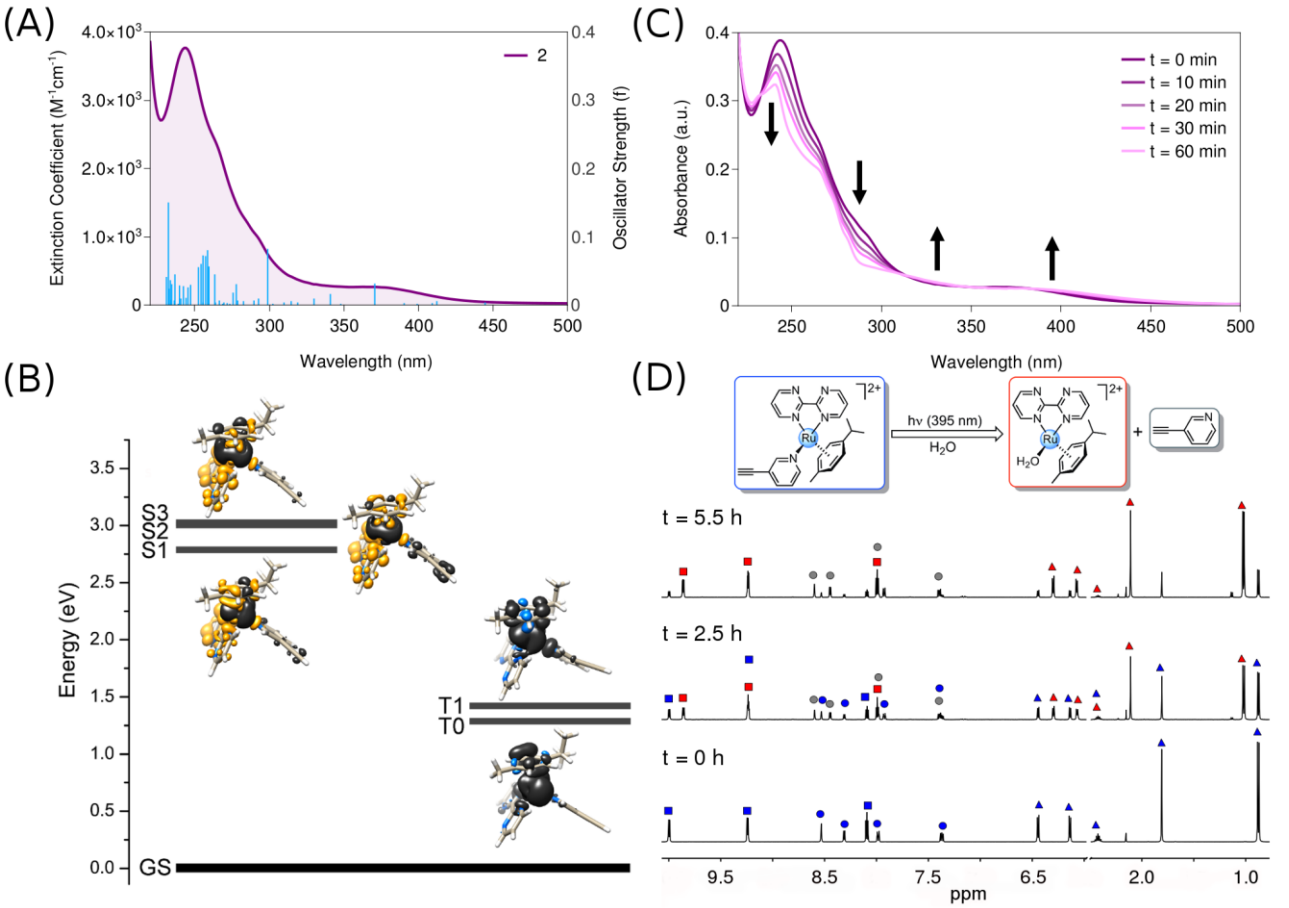

Figure 2. (A) UV-vis absorption spectrum of **2** in aqueous solution (95:5 H_2O:DMSO); blue vertical bars represent singlet-singlet TD-DFT transitions (see Table S2). (B) Singlet and triplet energy level diagram with EDDMs (singlets) and spin density surfaces (triplets) for **2**. In the EDDMs, black indicates a decrease in electron density while yellow indicates an increase. Time course photolysis reactions for **2** in aqueous solution (95:5 D_2O:DMSO-d_6) upon 395-nm excitation (15 mW·cm^{-2}) followed by (C) UV-vis and (D) ^{1}H NMR spectroscopy. ^{1}H NMR: **2** (blue), [(η^6-*p*-cym)Ru(bpm)(H_2O)]$^{2+}$(red) and free 3-ethynylpyridine(grey); ■ = bpm, ▲= *p*-cym, ● = 3-ethynylpyridine.

Near infrared Photochemisty using UCNPs

Photochemistry of 3, 4 and UCNP@4 under visible and NIR light excitation. Initially, the behaviour of clicked complexes **3** and **4** were verified and compared with their analogues **1** and **2** in the dark and under visible light conditions. NMR and UPLC-MS (Figure 3, S20-23) show that indeed, **3** and **4** react as the precursors **1** and **2**, both undergoing photodissociation of the P-Trz-Py ligand upon excitation at 395 nm. Addition of a GMP excess to irradiated solutions of **3** and **4** results in the formation of the adducts [(η^6-*p*-cym)Ru(bpy)(GMP)]$^{2+}$ and [(η^6-*p*-cym)Ru(bpm)(GMP)]$^{2+}$ after 12 hours of incubations at room temperature (Figure S24-27). Next, we selected **4** to perform decoration of UCNPs because of the slightly higher photodissociation yield of bpm complexes with respect to their bpy analogues.

For anchoring of **4** to UCNPs, we first synthesized core@shell $NaYF_4$:Yb^{3+}/Tm^{3+}(30/0.5%)@$NaYF_4$ nanoparticles by thermal decomposition as previously described by several groups (Experimental and Supporting Information sections).[17,49,50] UCNPs were thoroughly characterized by TEM, XPS, FTIR and emission spectroscopy (Figure S28–S32). TEM images of the core@shell UCNPs show uniform size and shape (diameter 37 nm, Figure 4A).

Functionalization with **4** was achieved as described in Scheme 1B and did not cause any observable change to the nanoparticles, rather TEM images of aqueous solution of **UCNP@4** showed an improved dispersion and lower aggregation compared to the core-only and core@shell UCNPs
capped with oleic acid. We obtained a rough estimate of the complex grafting density onto UCNPs by UV-vis spectroscopy following a procedure described previously by Branda.[51] Assuming a particle density of 4.2 $g \cdot cm^{-3}$ and a diameter of 36.9 nm, the **4**/UCNP ratio is approximately 3000 (3.5% wt). In THF, UCNPs display the typical upconversion emission of Tm^{3+} ions (Figure 4) with peaks at 345 and 360 nm ($^3P_0 \rightarrow {}^3F_4$ and $^1D_2 \rightarrow {}^3H_6$), 450 and 475 nm ($^1D_2 \rightarrow {}^3F_4$ and $^1G_4 \rightarrow {}^3H_6$), 645, 690 and 720 nm ($^1G_4 \rightarrow {}^3F_4$ and $^3F_3 \rightarrow {}^3H_6$) and at 800 nm ($^3H_4 \rightarrow {}^3H_6$). Photoluminescence studies confirm that core@shell NPs present higher emission profile compared to their core counterparts, especially in the UV-blue region of the spectrum (Figure S32). The undoped $NaYF_4$ shell is essential to improve
the efficiency of the upconversion process as it reduces non-radiative decay due to solvent and capping ligands.[49]

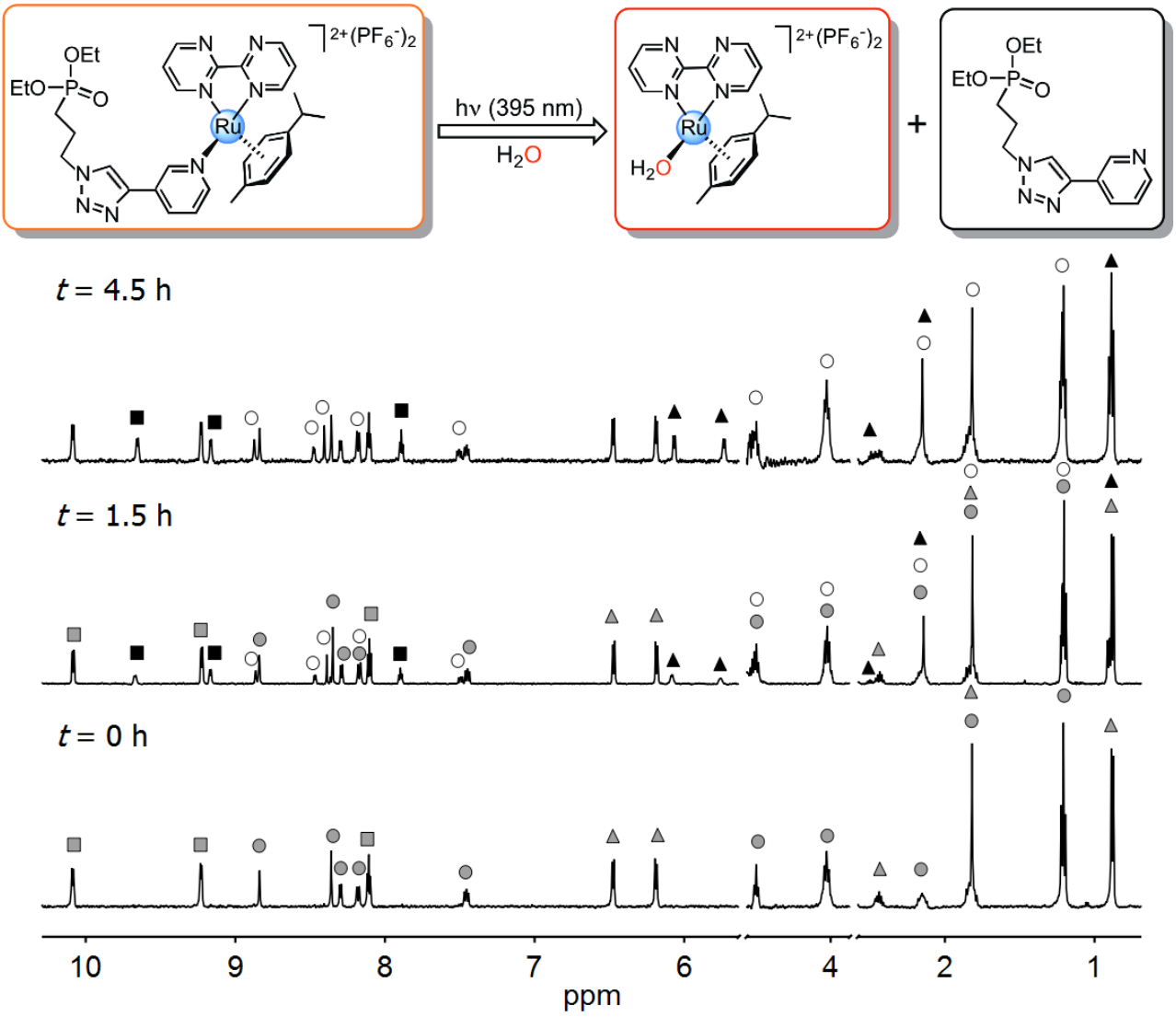

Figure 3. Photolysis time course for **4** in aqueous solution (95:5 H_2O:DMSO-d_6) upon 395 nm (15 $mW \cdot cm^{-2}$) followed by ^1H NMR. ^1H NMR: **4** (orange), $[(\eta^6\text{-}p\text{-cym})Ru(bpm)(H_2O)]^{2+}$ (red) and free P-Trz-Py (black); ■ = bpm, ▲= *p*-cym, ● = P-Trz-Py.

As we had demonstrated in a previous work,[17] such improvement is key to maximize the overlap between the emission spectrum of UCNPs and the absorption spectrum of metal complexes (Figure 4B). No significant changes in UCNPs luminescence was detected once the particles were treated with

As we had demonstrated in a previous work,[17] such improvement is key to maximize the overlap between the emission spectrum of UCNPs and the absorption spectrum of metal complexes (Figure 4B). No significant changes in UCNPs luminescence was detected once the particles were treated with hydrochloric acid solutions to remove the oleic acid, thus to favour the interaction with the phosphonic acid group of (activated) **4**. Surface modification was confirmed firstly by the colour of the UCNPs which became pale orange, and then by UV-vis of **UCNP@4** suspended in aqueous solution and by X-ray photoelectron spectroscopy (XPS). The UV-vis spectrum of **UCNP@4** (Figure 4B) exhibits the absorption profile of the complex with bands at 261 nm and 370 nm. Notably, the spectrum shows the characteristic band of the dopant ion Yb^{3+} at 980 nm.

Aqueous solutions of **4** and **UCNP@4** were deposited onto titanium supports for XPS measurements (Figure 4C and 4D and Figures S33 and S34). The expected Ru and P peaks for the Ru^{2+} ion and the phosphonic group of the ligand were observed in both samples, however dramatic difference appeared in the P $2p_{3/2}$ and $2p_{1/2}$ region. In particular, the protonation state of the phosphonic group was clearly different in the case of **UCNP@4** compared to **4**. The former showed a much greater proportion of $R–PO_3^{2-}$ *versus* $R–PO(OH)_2$ groups (90:10 for **UCNP@4** and 33:67 for **4**), in agreement with the formation of electrostatic interactions between the phosphonic group of the complex and the surface of the UCNPs.

Therefore, we investigated the effects of NIR light on **UCNP@4** in aqueous solution, irradiating at 980 nm and monitoring the course of photoreaction by ^1H NMR. This was possible despite ^1H NMR of **UCNP@4** has reduced resolution due to the intrinsic paramagnetism of UCNPs.

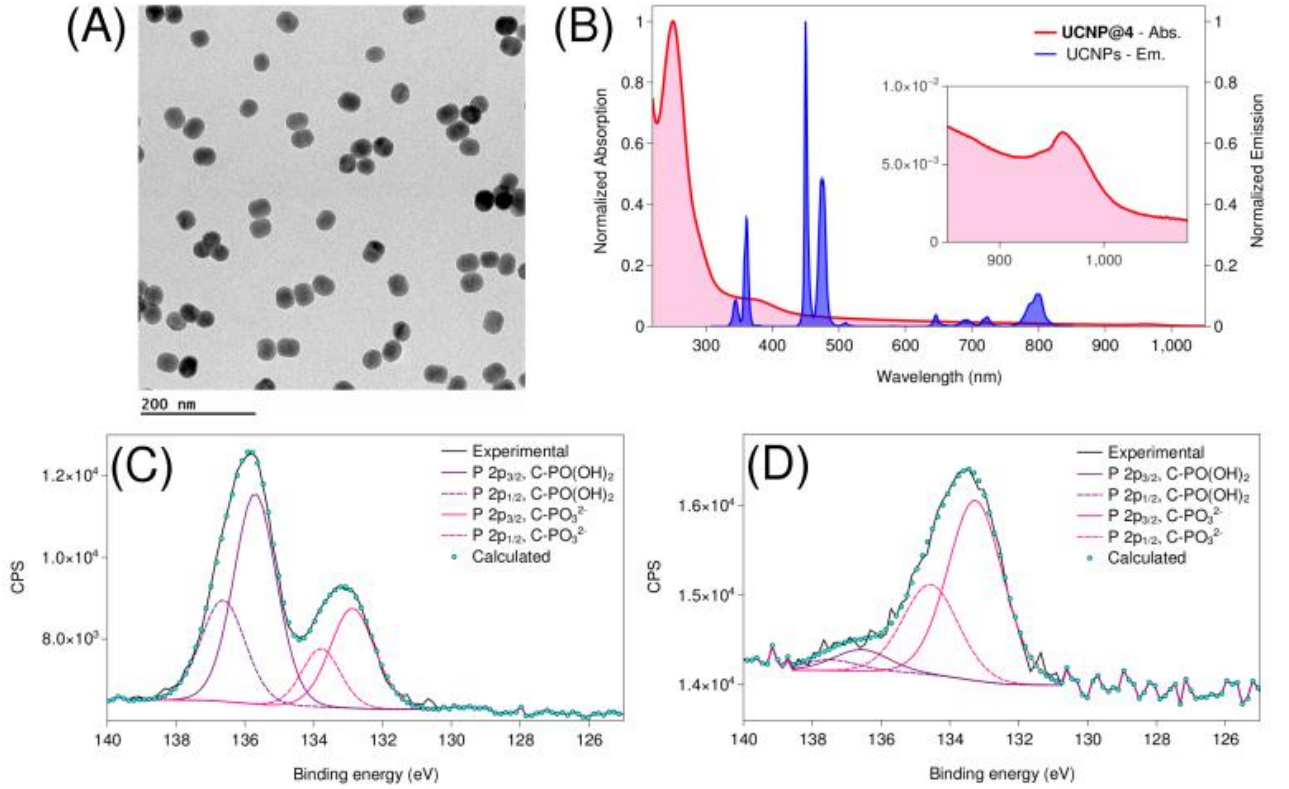

Figure 4. (A) TEM image of **UCNP@4** . (B) Overlap between the normalized absorption (violet) and emission (blue) spectrum of **UCNP@4** of core@shell UCNPs (THF) upon excitation at 980 nm (15 $W \cdot cm^{-2}$); Inset: zoom in the 900–1000 nm range of the absorption of **UCNP@4** in aqueous solution. P $2p_{3/2}$, $2p_{1/2}$ XPS spectra of (C) **4** and (D) **UCNP@4**

Remarkably, NMR spectra of NIR-irradiated **UCNP@4** display changes in signal pattern (Figure 5) resembling the ones observed for **4** under 395-nm excitation, ultimately confirming the formation of $[(\eta^6\text{-}p\text{-cym})Ru(bpm)(H_2O)]^{2+}$. Moreover, UPLC-MS experiments consistently show optimal agreement in retention time and m/z values for irradiated solution of **4** (395 nm, Figure S21) and **UCNP@4** (980 nm, Figure S35).

The aqua photoproduct generated by NIR light at the UCNP surface reacts with GMP to afford the adduct $[(\eta^6\text{-}p\text{-cym})\text{Ru(bpm)(GMP)}]^{2+}$ (as confirmed by NMR and UPLC-MS, Figure S36 and S37), hence demostrating the reactivity of Ru(II)-complexes towards biological targets can be triggered by low-energy photons.

Control experiments indicate that **UCNP@4** is stable and does not undergo ligand dissociation in dark, while **4** (and **2**) does not photoreact when irradiated by NIR light for several hours (Figure S38 and S39).

Photochemical efficiency in these hybrid systems still needs to be improved for more advanced applications; however combination of UCNPs optical features with their multimodal imaging capability can open new intriguing opportunities for innovative application in theranostics.

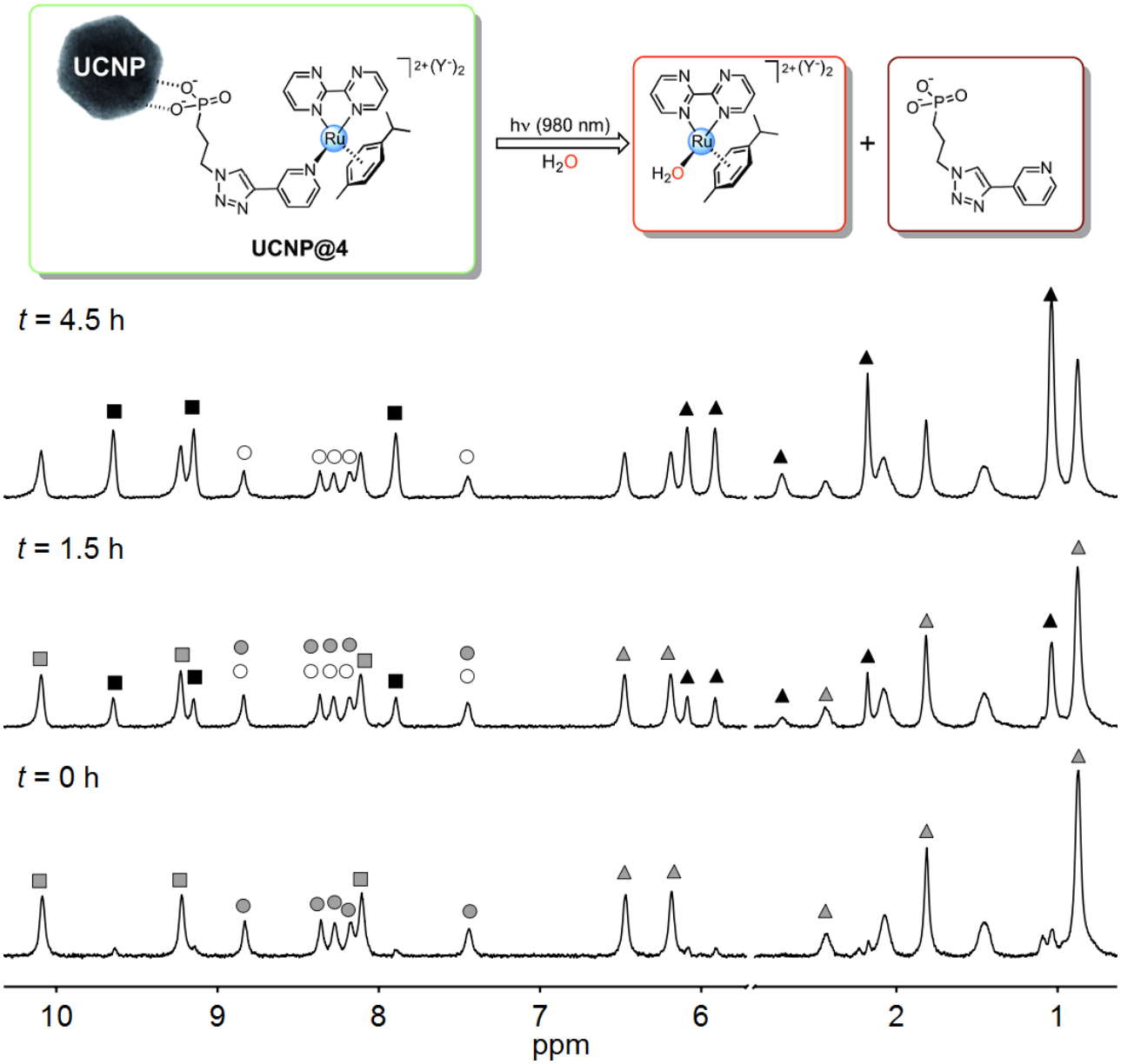

Figure 5. Photolysis time course for **UCNP@4** in aqueous solution upon 980-nm excitation (8.1 $W \cdot cm^{-2}$) followed by ^1H NMR. ^1H NMR: **UCNP@4** (green), P-Trz-Py (brown) and $[(\eta^6\text{-}p\text{-cym})\text{Ru(bpm)(H}_2\text{O)}]^{2+}$ (red); ■ = bpm, ▲= *p*-cym, ● = P-Trz-Py.

Conclusions

Our work reports on the synthesis of two new photoactivatable Ru-arene complexes (**1** and **2**) and the thorough characterization of their structural and photochemical proprieties. In addition, we demonstrated click chemistry is a valuable strategy to directly introduce a phosphonate group on complexes **1** and **2**, by

exploiting the alkyne function on the 3-ethynylpyridyl ligand coordinated to their Ru centres. As in the case of their precursors, the so-obtained derivatives (**3** and **4**) selectively release the pyridyl ligand under direct light excitation of their lowest-energy absorption band. Moreover, phosphonate groups on **3** and **4** confer these complexes high affinity for the surface of core@shell $NaYF_4$:Yb/Tm@$NaYF_4$ upconverting nanoparticles.

Notably, we found ligand photodissociation and GMP coordination is triggered under 980-nm excitation when **4** is anchored on UCNPs (**UCNP@4**), providing to the best our knowledge the first example of remote near infrared photoactivation of a Ru(II) arene model prodrug.

Although UCNPs are intensively investigated for medical application, research into their combination with coordination compounds is still very limited. The approach we proposed in the paper is of general applicability both in terms of synthetic and photoactivation strategy. The 3-ethynylpyridyl ligand is indeed a convenient candidate to perform click chemistry reactions in proximity of transition metal centres. Furthermore, the aliphatic arm of the azido-phosphonate ligand can be opportunely changed to modify the distance between the UCNPs and photoactivatable complexes and perhaps modulate their photochemistry.

In conclusions, our proof of concept study demonstrates UCNPs are convenient platforms for the use of deep-penetrating NIR light in the activation of anticancer metal complexes and *in situ* generation of active species.

Experimental Section

Materials

$RuCl_3 \cdot 3H_2O$ (99%) was purchased from Precious Metals Online (PMO Pty Ltd) and used as received. 2,2'-bipyrimidine (bpm) (97%), 2,2'-bipyridine (bpy) (≥ 99%), silver nitrate ($AgNO_3$) (≥ 99%), potassium hexafluorophosphate (KPF_6) (98%), 3-ethynylpyridine (98%), yttrium(III) acetate hydrate (99.9%), ytterbium(III) acetate tetrahydrate (99.9%), thulium(III) acetate hydrate (99.9%), 1-octadecene (technical grade, 90%), oleic acid (technical grade, 90%), sodium hydroxide (≥ 97%), ammonium fluoride (98%), iron(III) chloride (97%), potassium oxalate monohydrate (99%), sodium azide (≥ 95%), guanosine 5′-monophosphate disodium salt hydrate(≥ 99%). All solvents were obtained from Sigma-Aldrich and used as received.

Synthesis of Ruthenium Complexes

The dimer $[(\eta^6\text{-}p\text{-cym})RuCl_2]_2$ and the Ru^{II} complexes $[(\eta^6\text{-}p\text{-cym})Ru(bpy)Cl][PF_6]$ and $[(\eta^6\text{-}p\text{-cym})Ru(bpm)Cl][PF_6]$ were prepared based on literature methods.[39,40,41] The Ru^{II} pyridinato complexes **1**–**4** were prepared based on previously reported methodology with some modifications.[42]

Synthesis of [(η6-p-cym)Ru(bpy)(m-CCH-Py)][(PF)6]2 (1). An aluminium-foil-covered round bottom flask was charged with $[(\eta^6\text{-}p\text{-cym})Ru(bpy)Cl][PF_6]$ (500 mg, 1.2 mmol), in a 1:1 mixture of MeOH/H_2O (50 mL). $AgNO_3$ (0.2 g, 1.175 mmol) was then added and the reaction mixture stirred at ambient temperature for 18 h. The solution turned to light yellow and the off-white AgCl precipitate was filtered off. To the clear yellow solution of $[(\eta^6\text{-}p\text{-cym})Ru(bpy)(H_2O)]^{2+}$, 3-ethynylpyridine (620 mg, 6 mmol) was added to give a dark red solution. The reaction mixture was heated at 40 °C for 18 hours and KPF_6 (1.3 g, 7.2 mmol) was added after cooling. The precipitate that formed was dissolved by the addition of acetone to give a clear solution. This was filtered and the volume reduced until the onset of precipitation on the rotary evaporator, and left to evaporate slowly at ambient temperature to afford yellowish flakes. These were collected by filtration, washed with methanol and ether and dried in air.

Yield 330 mg, 35%; ^{1}H NMR (500 MHz, D_2O) δ=0.82 (d, ^3J(H,H)=6.9 Hz, 6H), 1.77 (s, 3H), 2.41 (spt, ^3J(H,H)=7.0 Hz, 1H), 5.99 (d, ^3J(H,H)=6.4 Hz, 2H), 6.40 (d, ^3J(H,H)=6.5 Hz, 2H), 7.30 (dd, ^3J(H,H)=8.0, 5.9 Hz, 1H), 7.86 (td, ^3J(H,H)=7.3, 5.7, 2H), 7.93 (dt, ^3J(H,H)=8.1, 1.5 Hz, 1H), 8.22 (td, ^3J(H,H)=7.9, 1.4 Hz, 2H), 8.30 (m, 3H), 8.51 (s, 1H), 9.64 ppm (d, ^3J(H,H)=5.0 Hz, 2H). In the ^{1}H NMR (D_2O), resonance of the proton of the alkyn group is overlapped by the residual water signal. In DMSO-d_6, it resonates at 4.73 ppm (s, 1H). ^{13}C NMR (125 MHz, DMSO-d_6) δ=17.89, 22.17, 30.56, 78.51, 84.94, 87.51, 92.48, 103.68, 108.76, 122.04, 125.15, 127.09, 129.47, 141.80, 143.29, 152.84, 155.07, 155.38, 156.69 ppm. FTIR (KBr

pellet) ν_{max} (cm^{-1}): 3300, 1580, 1410, 840, 560; ESI-MS: *m/z* (H_2O/MeOH), $[C_{27}H_{27}N_3RuPF_6]^+$ expected: 640.30, found: 640.09; elemental analysis calcd (%) for $C_{27}H_{27}F_{12}N_3P_2Ru$: C 41.34, H,, 3.47, N 5.36; found: C 40.94, H 3.12, N 5.08.

Synthesis of [(η6-p-cym)Ru(bpm)(m-CCH-Py)][(PF)6]2 (2). Complex **2** was synthesized using the procedure described above for **1**, using the [(η^6-*p*-cym)Ru(bpm)Cl][PF_6] precursor (200 mg, 0.48 mmol). Yield: (120 mg, 32%); ^{1}H NMR (500 MHz, D_2O) δ=0.88 (d, ^3J(H,H)=6.9 Hz, 6H), 1.81 (s, 3H), 2.43 (spt, ^3J(H,H)=7.0 Hz, 1H), 6.14 (d, ^3J(H,H)=6.5 Hz, 2H), 6.44 (d, ^3J(H,H)=6.5 Hz, 2H), 7.37 (dd, ^3J(H,H)=8.0, 5.8 Hz, 1H), 7.98 (dt, ^3J(H,H)=8.0, 1.5 Hz, 1H), 8.09 (dd, ^3J(H,H)=5.8, 4.9 Hz, 2H), 8.31 (d, ^3J(H,H)=5.8 Hz, 1H), 8.53 (s, 1H), 9.24 (dd, ^3J(H,H)=4.8, 1.9 Hz, 2H), 10.00 ppm (dd, ^3J(H,H)=5.8, 1.9 Hz, 2H). In the ^{1}H NMR (D_2O), the proton of the alkyn group is overlapped by the residual water signal. In DMSO-d_6, it resonates at 4.72 ppm (s, 1H). ^{13}C NMR (125 MHz, DMSO-d_6) δ=17.74, 22.18, 30.41, 78.79, 86.07, 87.28, 90.77, 106.33, 107.61, 122.01, 126.01, 126.91, 143.04, 153.44, 155.97, 160.84, 161.47, 164.10 ppm. FTIR (KBr pellet) ν_{max} (cm^{-1}): 3300, 1580, 1410, 840, 560; ESI-MS: *m/z* (H_2O/MeOH), $[C_{25}H_{25}N_5RuPF_6]^+$ expected: 642.28 , found: 642.08; elemental analysis calcd (%) for $C_{25}H_{25}F_{12}N_5P_2Ru$: C 38.18, H 3.20, N 8.90; found: C 37.59, H 3.04, N 8.71.

Synthesis of diethyl-3-azidopropyl phosphonate. The preparation of the azido-ligand for click chemistry is based on the procedure reported by A. K. Garrell and coworkers.[44] The (3-bromopropyl) phosphonic acid diethyl ether (5 mL, 26.02 mmol) was dissolved in acetone (25 mL) dried by passing through neutral alumina. To this, NaN_3 (2.6 g, 40.4 mmol) was added and the reaction mixture heated under reflux for 18 h. The reaction mixture was then cooled and was filtered through celite and washed several times with acetone. The solvent was taken off under rotary evaporation to leave a clear yellowish oil.

Yield 5.81 g, quantitative; ^{1}H NMR (500 MHz DMSO-d_6) δ=1.24 (t, ^3J(H,H)= 7.1 Hz, 6H), 1.78 (m, 4H), 3.41 (t, ^3J(H,H)= 6.6 Hz, 2H), 4.00 ppm (m, 4H); ^{31}P NMR (200 MHz, DMSO-d_6) δ=30.9 ppm; FTIR (KBr pellet) ν_{max} (cm^{-1}): 3400, 3000, 2100, 1240, 1050, 960.

Synthesis of [(η6-p-cym)Ru(bpy)(P-Trz-Py)][(PF)6]2 (3) (P-Trz-Py = [3-(1-Pyridin-3-yl-[1,2,3]triazol-4-yl)-propyl]-phosphonic acid diethyl ester). To a solution of [(η^6-p-cym)Ru(bpy)(*m*-CCH-Py)][$(PF)_6$]$_2$ (**1**) (50 mg, 0.064 mmol) in THF/H_2O (4:1, 5 mL) 50% mol $CuSO_4$ (8 mg, 0.032 mmol), 50% mol sodium ascorbate (6.3 mg, 0.032 mmol) and diethyl-3-azidopropyl phosphonate (14.4 mg, 0.064 mmol) were added and the reaction mixture heated at 60 °C for 72 h. KF_6 (9.5 g, 52 mmol) in H_2O (30 mL) was then added and the reaction mixture placed in a separating funnel and extracted with dichloromethane (3 times, 10 mL) to give a reddish dilution. This was dried over $MgSO_4$ and the solvent taken off in a rotary evaporator to give an oily product. This was dissolved in methanol, an additional KPF_6 (2 g) was added and the product was precipitated by the addition of diethyl ether. The solid was collected by decanting the diethyl ether and the residue re-dissolved in dichloromethane and the precipitated salt was filtered off. The red solid obtained was dried in air.

Yield (25 mg, 41%); ^{1}H NMR (500 MHz, D_2O) δ=0.83 (d, ^3J(H,H)= 6.9 Hz, 6H), 1.19 (t, ^3J(H,H)= 7.1 Hz, 6H), 1.82 (m, 5H), 2.15 (m, 2H), 2.44 (stp, ^3J(H,H)= 6.8 Hz, 1H), 4.02 (m, 4H), 4.49 (t, ^3J(H,H)= 6.7 Hz, 2H), 6.05 (d, ^3J(H,H)= 6.3 Hz, 2H), 6.44 (d, ^3J(H,H)= 6.3 Hz, 2H), 7.40 (dd, ^3J(H,H)= 8.1, 5.8 Hz, 1H), 7.89 (t, ^3J(H,H)= 7.2 Hz, 2H), 8.14 (d, ^3J(H,H)= 8.0 Hz, 1H), 8.22 (t, ^3J(H,H)= 7.9 Hz, 2H), 8.29 (m, 4H), 8.79 (s, 1H), 9.72 (d, ^3J(H,H)= 6.0 Hz, 2H) ppm; ^{13}C NMR (125 MHz, DMSO-d_6) δ=16.73, 17.94, 21.54, 22.21, 23.77, 30.61, 50.21, 61.59, 85.06, 92.33, 104.02, 108.57, 124.05, 125.15, 127.61, 129.51, 130.03, 136.78, 141.74, 141.80, 148.54, 152.37, 155.27, 156.71 ppm; ^{31}P NMR (200 MHz, DMSO-d_6) δ=30.4 ppm; ESI-MS *m/z* (H_2O/MeOH), $[C_{34}H_{43}O_3N_6PRuPF_6]^+$ expected: 861.45, found: 861.18 .

Synthesis of [(η6-p-cym)Ru(bpm)(P-Trz-Py)] [(PF)6]2 (4) (P-Trz-Py = [3-(1-Pyridin-3-yl-[1,2,3]triazol-4-yl)-propyl]-phosphonic acid diethyl ester). Complex **4** was synthesized using the procedure described above for **3**, starting with [(η^6-p-cym)Ru(bpm)(*m*-CCH-Py)][$(PF)_6$]$_2$ (50 mg, 0.06 mmol)). Yield: (15 mg, 23%); ^{1}H NMR (500 MHz, D_2O) δ=0.89 (d, ^3J(H,H)= 6.9 Hz, 6H), 1.21 (t, ^3J(H,H)= 7.1 Hz, 6H), 1.82 (m, 5H), 2.16 (m, 2H), 2.45 (stp, ^3J(H,H)= 6.8 Hz, 1H), 4.03 (m, 4H), 4.50 (t, ^3J(H,H)= 6.8 Hz, 2H), 6.19 (d, ^3J(H,H)= 6.4 Hz, 2H), 6.48 (d, ^3J(H,H)= 6.4 Hz, 2H), 7.46 (dd, ^3J(H,H)= 8.1, 5.8 Hz, 1H), 8.11 (dd, ^3J(H,H)= 5.9, 4.8 Hz,

2H), 8.18 (dt, ^3J(H,H)= 8.1, 1.6 Hz, 1H), 8.30 (d, ^3J(H,H)= 5.7 Hz, 1H), 8.36 (s, 1H), 8.84 (s, 1H), 9.23 (dd, ^3J(H,H)= 4.9, 1.9 Hz, 2H), 10.09 ppm (dd, ^3J(H,H)= 5.9, 1.9 Hz, 2H); ^{13}C NMR (125 MHz, DMSO-d_6,) δ=16.73, 17.80, 22.24, 22.66, 23.80, 30.48, 50.35, 61.62, 86.19, 90.64, 106.66, 107.47, 123.96, 126.05, 127.53, 130.07, 137.58, 141.97, 149.52, 152.92, 160.78, 161.54, 164.13 ppm; ^{31}P NMR (200 MHz, DMSO-d_6) δ=30.4 ppm. ESI-MS *m/z* (H_2O/MeOH), $[C_{32}H_{41}O_3N_8PRuPF_6]^+$ expected: 863.42, found: 863.17.

Synthesis of UCNPS

The core@shell $NaYF_4$:Yb(30%)/Tm(0.5%)@$NaYF_4$ nanoparticles were synthesized in two steps by thermal decomposition, as previously reported by us[16] and others.[45,46] The oleate-coated core $NaYF_4$:Yb^{3+}/Tm^{3+} (30/0.5 %) nanoparticles were first synthesized employing acetate salt of rare earth elements (Y, Yb, Tm) in oleic acid and octadecene solution. Subsequently, an undoped $NaYF_4$ protective shell was grown around on the surfaces of the core NPs, using the same synthetic procedure. Full synthetic details and characterization (IR, XPS, TEM, optical proprieties) of the NPs is reported in the Supporting Information.

Synthesis of the adduct UCNP@4

Both **3** and **4** selectively photodissociate the **P-Trz-Py** ligand upon irradiation at 400 nm. However, **4** was selected for the functionalization of UCNPs (Scheme 2) and NIR photolysis studies because its analogue bpm derivative **2** displayed slight higher photodissociation yield compared to the bpy derivative **1**.

Deprotection of [(η^6-p-cym)Ru(bpm)(P-Trz-Py)][$(PF)_6$]$_2$ (4). We followed a similar procedure to the reported one for the deprotection of diethyl-3-azidopropyl phosphonate to 3-azido propyl phosphoric acid.[47] An aluminium-foil-covered round-bottom flask was charged with 2.5 mg of [(η^6-p-cym)Ru(bpm)(P-Trz-Py)][$(PF)_6$]$_2$ (**4**) in CH_2Cl_2 (anhydrous), (1 mL) obtaining a yellow solution. Trimethylsilyl bromide (TMSBr) was added (c.a. 10 drops) to the flask. Instantaneously the reaction solution changed from transparent to cloudy. After the end of the addition, the reaction mixture was maintained under stirring overnight at ambient temperature. Afterwards, the solvent was removed under gentle nitrogen flow to give a yellow precipitate.

Preparation of oleate-free UCNPs. The preparation was performed following literature procedure reported by N. Bogdan et al.[52] Briefly, in round-bottom flask 50 mg of core@shell $NaYF_4$:Yb(30%)/Tm(0.5%)@$NaYF_4$ were suspended in H_2O (5 mL). The pH of the mixture was adjusted to 4 using 0.1 M HCl solution and the suspension was then stirred for 2 h at ambient temperature. Afterwards, the oleate-free UCNPs were purified from the released oleic acid *via* extraction with diethyl ether (3 times, 5 mL). The product (ca. 30 mg) was dried at ambient temperature overnight.

Functionalization of oleate-free UCNPs with 4. In an aluminium-foil-covered round-bottom flask, complex **4** deprotected (2.5 mg) was mixed with oleate-free core@shell $NaYF_4$:Yb/Tm@$NaYF_4$ (10 mg) and suspended in H_2O (1.5 mL). The suspension was stirred overnight at ambient temperature. The reaction mixture was then lyophilized. The yellow powder obtained was washed several times with ethanol and precipitated by centrifugation (10000 rpm for 5 min) to remove excess of Ru complex. The **UCNP@4** (ca. 6 mg) was dried at ambient temperature overnight.

^{1}H NMR (500 MHz, D_2O) δ=0.87 (6H), 1.81 (3H), 2.16 (2H), 2.43 (1H), 4.47 (2H), 6.18 (2H), 6.47 (2H), 7.44 (1H), 8.11 (2H), 8.18 (1H), 8.27 (1H), 8.36 (1H), 8.83 (1H), 9.22 (2H), 10.09 ppm (2H). All proton signals of **UCNP@4** were broader than those of **4**. Lose of multiplicity is due to the paramagnetic nature of the UCNPs. In addition, four aliphatic protons relative to the propyl chain of the phosphonic acid group gave signals too broad to be observed (previously falling in at δ_H 4.03 ppm in complex **4**), due to their proximity to the surface of UCNPs.

Photolysis experiments

Photoirradiation of Ru complexes at 395 nm. Aqueous solutions of **1**–**4** were irradiated at 395 nm with the Prizmatix LED Multi-Wavelength MWLLS-11 source (15 mW·cm^{-2}) at ambient temperature. The progress of the photoreaction was followed by either ^{1}H NMR or UV-vis spectroscopies. Finally, the nature of the photoproducts was also analysed by UPLC-MS.

Photoirradiation of 4 and UCNP@4 at 980 nm. Aqueous solutions of **4** and **UCNP@4** were irradiated under 980 nm light using a BWT diode laser DS3-11312-110. Complex **4** (150 µM, 400 µL) and **UCNP@4**

(10 mg/mL, 400 µL) solutions were irradiated for 7 h (8.8 $W \cdot cm^{-2}$) and 5.5 h (8.1 $W \cdot cm^{-2}$), respectively. The progress of photoreaction was followed by ^{1}H NMR measurements. Before ^{1}H NMR measurements, solutions of **UCNP@4** were centrifuged (6000 rpm, 5 min) to improve the quality of the NMR spectra. Finally, the nature of the photoproducts was also analysed by UPLC-MS.

The output power density of all light sources employed was measured by an optical power meter (Ophir Photonics PD300-3W).

NMR Spectroscopy. ^{1}H, ^{13}C, ^{31}P NMR spectra of the various samples in deuterated solvents (D_2O or DMSO-d_6) were acquired using standard pulse programson an AVANCE III Bruker 500 NMR spectrometer. Chemical shifts were reported in parts-per-million (δ, ppm) and referenced to the residual solvent peak.

X-ray Crystallography. Diffraction data for **1** and **2** was obtained using an Agilent Super Nova Mo-diffractometer coupled with CCD area detector. All work was conducted at 100 K using an Agilent 700 Cryosystem Cooler fed with liquid nitrogen. Full-matrix least-squares refinements based on F2 were performed using SHELXL-97 and the structures were solved by direct methods. The rest of the hydrogen atoms were located by riding model. The crystallographic details of **1** and **2** have been deposited in the Cambridge Crystallographic Data Centre under the accession numbers 1055609 and 1055610, respectively.

Fourier-transform Infrared (FTIR) Spectroscopy. FTIR spectra of **1**, **2**, core-$NaYF_4$:Yb/Tm, core@shell-$NaYF_4$:Yb/Tm@$NaYF_4$ and oleate-freecore@shell-$NaYF_4$:Yb/Tm@$NaYF_4$ were recorded on a Nicolet FTIR 6700 spectrometer as KBr disk.

UV-vis Absorption Spectroscopy. UV-vis experiments of Ru complexes and **UCNP@4** were performed in H_2O using a Varian Cary 5000 spectrophotometer.

Emission Spectroscopy. The emission spectra of UCNPs dispersions (in THF or H_2O) were obtained under 980 nm excitation (15 $W \cdot cm^{-2}$) with a 980 nm laser diode (CNI, MDL-N-980) coupled with a Fluorometer Fluorolog-TSPC (Horiba).. The laser power density was measured as described above.

Transmission Electron Microscopy (TEM). TEM images were collected on core-$NaYF_4$:Yb/Tm, core@shell-NaYF4:Yb/Tm@$NaYF_4$ and **UCNP@4** samples using a JEOL JEM-1400 PLUS-HC microscope operating at 120 kV. A small amount of the sample was dispersed in 1 mL of solvent (H_2O or THF) to give an approximate 0.5 mg/mL solution. One drop (3 µL) of the resulting solution was allowed to evaporate on a carbon film supported on a 300 mesh copper grid (3 mm in diameter).

X-Ray Photoelectron Spectroscopy (XPS). XPS data of **4** and **UCNP@4** were acquired employing a SPECS Sage HR 100 spectrometer with a non-monochromatic X-ray source Magnesium Kα line of 1253.6 eV energy and a power applied of 250 W and calibrated using the $3d_{5/2}$ line of Ag with a full width at half maximum (FWHM) of 1.1 eV. All measurements were made in an ultra-high vacuum (UHV) chamber at a pressure below $8 \cdot 10^{-8}$ mbar. Samples were measured on titanium surfaces.

Ultra PerformanceLiquid Chromatography-Mass Spectrometry (UPLC-MS). UPLC-MS measurements on **1**–**4** were performed by positive-ion electrospray ionization mass spectrometry (ESI-MS) LCT Premier XE from Waters (10000 FWHM) coupled to an Ultra Performance Liquid Chromatograph (UPLC). Samples were prepared in a H_2O/DMSO (95/5%) mixture. The analysis was achieved on an ACQUITY UPLC BEH C18 column (50 × 2.1 mm) using H_2O (0.1% formic acid)/MeOH as the mobile phase with a flow rate of 0.3 mL min^{-1}. The injection volume was 5 µL. The ESI source was employed in W-optics positive ionization scan mode with the capillary voltage at 2.5 kV. The temperatures of the source and desolvation were 120 ºC. The cone and desolvation gas flows were 50 and 600 L h^{-1}. The collision gas flow was 0.2 mL min^{-1} and collision energy of 15–18 V was operated. In the case of **UCNP@4**, the sample was sonicated and ultracentrifugated (10^5 rpm, 45 min) in order to eliminate possible aggregates and nanoparticles before the injection in the UPLC-MS.

Ligand Photodissociation Quantum Yield. The quantum yields (Φ) of ligand photodissociation were determined for **1** and **2** in H_2O upon excitation at 395 nm. UV-vis absorption spectroscopy was employed to quantify the formation of the photo-products as function of irradiation time (nmol/s). At the same time, ferrioxalate actinometer $K_3[Fe(C_2O_4)_3]$ was used to determine the photon flux (µmol/s) on the samples exposed to the Prizmatix LED Multi-Wavelength MWLLS-11 at 395 nm. Full account of details is shown in

the Supporting Information. The complex $K_3[Fe(C_2O_4)_3]$ was obtained following the procedure described by J. G. Carriazo.[53]

Computational Details. All calculations were performed with the Gaussian 09 (G09) program package,[54] employing the DFT and TD-DFT methods,[55,56] the Becke three-parameter hybrid functional,[57] and the Lee−Yang−Parr's gradient corrected correlation functional (B3LYP).[58] The solvent effect was included using the polarizable continuum model (PCM method)[59,60] with water as solvent. The LanL2DZ basis set[61] and effective core potential were used for the Ru atom and the 6-31G** basis set[62] was used for all the other atoms. The B3LYP/LanL2DZ/6-31G** combination was selected since it previously provided satisfactory results on similar ruthenium arene complexes.[35,36]

Geometry optimizations of ground states (S0) and lowest-lying triplet states (T0 and T1) for **1** and **2** were carried out without any symmetry constraints. The nature of all stationary points was verified via harmonic vibrational frequency calculations. No imaginary frequencies were found, indicating we had located minima on potential energy surfaces.

The UV-vis electronic absorption spectra were simulated by TD-DFT,[55,56] computing a total of 50 singlet excited states. The electronic distribution and the localization of the singlet excited states were visualized using electron density difference maps (EDDMs).

GaussSum 2.2.5[63] was used to simulate the theoretical UV–vis spectra and for extraction of EDDMs.[64,65] Molecular graphics images were produced using the UCSF Chimera package from the Resource for Biocomputing, Visualization, and Informatics at the University of California, San Francisco (supported by NIH P41 RR001081).[66] A full summary of the computational results is reported in the Supporting Information.

Acknowledgements

Our work in this area was supported by the Spanish Ministry of Economy and Competitiveness (grant CTQ2012-39315), the Department of Industry of the Basque Country (grant ETORTEK). L.S. and E.R. were supported by the MICINN of Spain with the Ramón y Cajal Fellowship RYC-2011-07787 and by the MC CIG fellowship UCnanomat4iPACT (grant no. 321791). We gratefully acknowledge IKERBASQUE for the Visiting Professor Fellowship to A.H. and members of the European COST Actions CM1105 and CM1403 for stimulating discussions. Marco Moller, Javier Calvo, Daniel Padró and Luis Yate are also kindly acknowledged for helping in the collection of experimental data. Moreover, technical and human support provided by SGIker (UPV/EHU, MINECO, GV/EJ, ERDF and ESF) is gratefully acknowledged.

Keywords: upconverting nanoparticles • photoactivation • ruthenium • nanoparticles • near infrared

References

[1] D. E. J. G. J. Dolmans, D. Fukumura, R. K. Jain, *Nat. Rev. Cancer* **2003**, *3*, 380–387.

[2] E. Fino, R. Araya, D. S. Peterka, M. Salierno, R. Etchenique, R. Yuste, *Front. Neural Circuits* **2009**, *3, art. n. 2*.

[3] M. A. Sgambellone, A. David, R. N. Garner, K. R. Dunbar, C. Turro, *J. Am. Chem. Soc.* **2013**, *135*, 11274–11282.

[4] U. Schatzschneider, *Eur. J. Inorg. Chem.* **2010**, *2010*, 1451–1467.

[5] E. Ruggiero, S. Alonso-de Castro, A. Habtemariam, L. Salassa, in *Struct. Bond.* **2015**, *165*, 69–108.

[6] N. J. Farrer, L. Salassa, P. J. Sadler, *Dalton Trans.* **2009**, 10690–10701.

[7] E. C. Glazer, *Isr. J. Chem.* **2013**, *53*, 391–400.

[8] D. Barolet, *Semin. Cutan. Med. Surg.* **2008**, *27*, 227–238.

[9] Z. Chen, W. Sun, H. J. Butt, S. Wu, *Chem. – Eur. J.* **2015**, *15*, 9165–9170.

[10] E. Wachter, D. K. Heidary, B. S. Howerton, S. Parkin, E. C. Glazer, *Chem. Commun. Camb. Engl.* **2012**, *48*, 9649–9651.

[11] M. J. Rose, P. K. Mascharak, *Inorg. Chem.* **2009**, *48*, 6904–6917.
[12] M. J. Rose, N. L. Fry, R. Marlow, L. Hinck, P. K. Mascharak, *J. Am. Chem. Soc.* **2008**, *130*, 8834–8846.
[13] J. V. Garcia, J. Yang, D. Shen, C. Yao, X. Li, R. Wang, G. D. Stucky, D. Zhao, P. C. Ford, F. Zhang, *Small* **2012**, *8*, 3800–3805.
[14] A. E. Pierri, P.-J. Huang, J. V. Garcia, J. G. Stanfill, M. Chui, G. Wu, N. Zheng, P. C. Ford, *Chem. Commun.* **2015**, *51*, 2072–2075.
[15] S. He, K. Krippes, S. Ritz, Z. Chen, A. Best, H.-J. Butt, V. Mailander, S. Wu, *Chem. Commun.* **2015**, *51*, 431–434.
[16] E. Ruggiero, A. Habtemariam, L. Yate, J. C. Mareque-Rivas, L. Salassa, *Chem. Commun.* **2014**, *50*, 1715–1718.
[17] E. Ruggiero, J. Hernandez-Gil, J. C. Mareque-Rivas, L. Salassa, *Chem. Commun.* **2015**, *51*, 2091–2094.
[18] S. Wu, H. J. Butt, *Adv. Mater.* **2015**.
[19] Z. Chen, S. He, H. J. Butt, S. Wu, *Adv. Mater.* **2015**, *27*, 2203–2206.
[20] S. He, K. Krippes, S. Ritz, Z. Chen, A. Best, H. J. Butt, V. Mailänder, S. Wu, *Chem. Commun.* **2015**, *51*, 431-434.
[21] M. Haase, H. Schäfer, *Angew. Chem. Int. Ed.* **2011**, *50*, 5808–5829.
[22] J. Zhou, Q. Liu, W. Feng, Y. Sun, F. Li, *Chem. Rev.* **2015**, *115*, 395–465.
[23] S. H. C. Askes, A. Bahreman, S. Bonnet, *Angew. Chem. Int. Ed.* **2014**, *53*, 1029–1033.
[24] Y. Sun, M. Yu, S. Liang, Y. Zhang, C. Li, T. Mou, W. Yang, X. Zhang, B. Li, C. Huang, et al., *Biomaterials* **2011**, *32*, 2999–3007.
[25] T. Cao, Y. Yang, Y. Sun, Y. Wu, Y. Gao, W. Feng, F. Li, *Biomaterials* **2013**, *34*, 7127–7134.
[26] J.-W. Shen, C.-X. Yang, L.-X. Dong, H.-R. Sun, K. Gao, X.-P. Yan, *Anal. Chem.* **2013**, *85*, 12166–12172.
[27] J. Zhou, Y. Sun, X. Du, L. Xiong, H. Hu, F. Li, *Biomaterials* **2010**, *31*, 3287–3295.
[28] L. Xiong, Z. Chen, Q. Tian, T. Cao, C. Xu, F. Li, *Anal. Chem.* **2009**, *81*, 8687–8694.
[29] S. K. Maji, S. Sreejith, J. Joseph, M. Lin, T. He, Y. Tong, H. Sun, S. W.-K. Yu, Y. Zhao, *Adv. Mater.* **2014**, *26*, 5632–5632.
[30] Y. Sun, W. Feng, P. Yang, C. Huang, F. Li, *Chem. Soc. Rev.* **2015**, *44*, 1509–1525.
[31] J. Zhou, Z. Liu, F. Li, *Chem. Soc. Rev.* **2012**, *41*, 1323–1349.
[32] G. Gasser, I. Ott, N. Metzler-Nolte, *J. Med. Chem.* **2011**, *54*, 3–25.
[33] Z. Adhireksan, G. E. Davey, P. Campomanes, M. Groessl, C. M. Clavel, H. Yu, A. A. Nazarov, C. H. F. Yeo, W. H. Ang, P. Dröge, U. Rothlisberger, P. J. Dyson, C. A. Davey, *Nat. Commun.* **2014**, *5*, 3462.
[34] M. Frik, A. Martínez, B. T. Elie, O. Gonzalo, D. Ramírez de Mingo, M. Sanaú, R. Sánchez-Delgado, T. Sadhukha, S. Prabha, J. W. Ramos, I. Marzo, M. Contel, *J. Med. Chem.* **2014**, *57*, 9995–10012.
[35] S. Betanzos-Lara, L. Salassa, A. Habtemariam, O. Novakova, A. M. Pizarro, G. J. Clarkson, B. Liskova, V. Brabec, P. J. Sadler, *Organometallics* **2012**, *31*, 3466–3479.
[36] S. Betanzos-Lara, L. Salassa, A. Habtemariam, P. J. Sadler, *Chem. Commun.* **2009**, 6622–6624.
[37] G. Ragazzon, I. Bratsos, E. Alessio, L. Salassa, A. Habtemariam, R. J. McQuitty, G. J. Clarkson, P. J. Sadler, *Inorg. Chim. Acta* **2012**, *393*, 230–238.
[38] J.-C. Boyer, M.-P. Manseau, J. I. Murray, F. C. J. M. van Veggel, *Langmuir* **2010**, *26*, 1157–1164.
[39] R. A. Zelonka, M. C. Baird, *Can. J. Chem.* **1972**, *50*, 3063–3072.
[40] M. A. Bennett, A. K. Smith, *J. Chem. Soc. Dalton Trans.* **1974**, 233–241.
[41] A. Habtemariam, M. Melchart, R. Fernández, S. Parsons, I. D. H. Oswald, A. Parkin, F. P. A. Fabbiani, J. E. Davidson, A. Dawson, R. E. Aird, et al., *J. Med. Chem.* **2006**, *49*, 6858–6868.

[3842] F. Wang, A. Habtemariam, E. P. L. van der Geer, R. Fernández, M. Melchart, R. J. Deeth, R. Aird, S. Guichard, F. P. A. Fabbiani, P. Lozano-Casal, et al., *Proc. Natl. Acad. Sci. U. S. A.* **2005**, *102*, 18269–18274.
[43] B. S. Uppal, A. Zahid, P. I. P. Elliott, *Eur. J. Inorg. Chem.* **2013**, *2013*, 2571–2579.
[44] B. C. Boren, S. Narayan, L. K. Rasmussen, L. Zhang, H. Zhao, Z. Lin, G. Jia, V. V. Fokin, *J. Am. Chem. Soc.* **2008**, *130*, 8923–8930.
[45] J.-C. Boyer, C.-J. Carling, S. Y. Chua, D. Wilson, B. Johnsen, D. Baillie, N. R. Branda, *Chem. – Eur. J.* **2012**, *18*, 3122–3126.
[46] L.-L. Li, P. Wu, K. Hwang, Y. Lu, *J. Am. Chem. Soc.* **2013**, *135*, 2411–2414.
[47] A. K. Tucker-Schwartz, R. L. Garrell, *Chem. – Eur. J.* **2010**, *16*, 12718–12726.
[48] M. Montalti, A Credi, L Prodi, M. T. Gandolfi, *Handbook of Photochemistry, Third Edition.* **2006**, CRC press.
[49] F. Vetrone, R. Naccache, V. Mahalingam, C. G. Morgan, J. A. Capobianco, *Adv. Funct. Mater.* **2009**, *19*, 2924–2929.
[50] C. J. Carling, F. Nourmohammadian, J. C. Boyer, N. R. Branda, *Angew. Chem. Int. Ed. Engl.* **2010**, *17*, 3782-3785.
[51] J.-C. Boyer, C.-J. Carling, B. D. Gates, N. R. Branda, *J. Am. Chem. Soc.* **2010**, *132*, 15766–15772.
[52] N. Bogdan, F. Vetrone, G. A. Ozin, J. A. Capobianco, *Nano Lett.* **2011**, *11*, 835–840.
[53] J. G. Carriazo, *Chemistry*, **2010**, *19*, 103–112.
[54] M. J. Frisch, G. W. Trucks, H. B. Schlegel, G. E. Scuseria, M. A. Robb, J. R. Cheeseman, G. Scalmani, V. Barone, B. Mennucci, G. A. Petersson, H. Nakatsuji, M. Caricato, X. Li, H. P. Hratchian, A. F. Izmaylov, J. Bloino, G. Zheng, J. L. Sonnenberg, M. Hada, M. Ehara, K. Toyota, R. Fukuda, J. Hasegawa, M. Ishida, T. Nakajima, Y. Honda, O. Kitao, H. Nakai, T. Vreven, J. A. Montgomery, Jr., J. E. Peralta, F. Ogliaro, M. Bearpark, J. J. Heyd, E. Brothers, K. N. Kudin, V. N. Staroverov, R. Kobayashi, J. Normand, K. Raghavachari, A. Rendell, J. C. Burant, S. S. Iyengar, J. Tomasi, M. Cossi, N. Rega, J. M. Millam, M. Klene, J. E. Knox, J. B. Cross, V. Bakken, C. Adamo, J. Jaramillo, R. Gomperts, R. E. Stratmann, O. Yazyev, A. J. Austin, R. Cammi, C. Pomelli, J. W. Ochterski, R. L. Martin, K. Morokuma, V. G. Zakrzewski, G. A. Voth, P. Salvador, J. J. Dannenberg, S. Dapprich, A. D. Daniels, Ö. Farkas, J. B. Foresman, J. V. Ortiz, J. Cioslowski, D. J. Fox, *Gaussian 09, Revision C.01;* Gaussian, Inc.: Wallingford, CT, **2009**.
[55] M. E. Casida, C. Jamorski, K. C. Casida, D. R. Salahub, *J. Chem. Phys.* **1998**, *108*, 4439–4449.
[56] R. E. Stratmann, G. E. Scuseria, M. J. Frisch, *J. Chem. Phys.* **1998**, *109*, 8218–8224.
[57] A. D. Becke, *J. Chem. Phys.* **1993**, *98*, 5648–5652.
[58] C. Lee, W. Yang, R. G. Parr, *Phys. Rev. B* **1988**, *37*, 785–789.
[59] M. Cossi, G. Scalmani, N. Rega, V. Barone, *J. Chem. Phys.* **2002**, *117*, 43–54.
[60] S. Miertuš, E. Scrocco, J. Tomasi, *Chem. Phys.* **1981**, *55*, 117–129.
[61] P. J. Hay, W. R. Wadt, *J. Chem. Phys.* **1985**, *82*, 270–283.
[62] A. D. McLean, G. S. Chandler, *J. Chem. Phys.* **1980**, *72*, 5639–5648.
[63] N. M. O'Boyle, A. L. Tenderholt, K. M. Langner, *J. Comput. Chem.* **2008**, *29*, 839–845.
[64] W. R. Browne, N. M. O'Boyle, J. J. McGarvey, J. G. Vos, *Chem. Soc. Rev.* **2005**, *34*, 641–663.
[65] M. Head-Gordon, A. M. Grana, D. Maurice, C. A. White, *J. Phys. Chem.* **1995**, *99*, 14261–14270.
[66] E. F. Pettersen, T. D. Goddard, C. C. Huang, G. S. Couch, D. M. Greenblatt, E. C. Meng, T. E. Ferrin, *J. Comput. Chem.* **2004**, *25*, 1605–1612.